Conductive Atomic Force Microscope Nanopatterning of Epitaxial Graphene on SiC(0001) in Ambient Conditions

*Justice M. P. Alaboson, Qing Hua Wang, Joshua A. Kellar, Joohee Park, Jeffrey W. Elam, Michael J. Pellin, and Mark C. Hersam**

Graphene has attracted significant attention in recent years for its extraordinary electronic, physical, optical, and magnetic properties.[1] In particular, epitaxial graphene (EG) grown on SiC substrates is a promising route towards realizing graphene-based electronics.[2–4] Control over the surface chemistry[5,6] and lithographic engineering of graphene are required for the fabrication of a wide range of devices and for incorporation with different electronic materials such as high-k dielectrics.[7,8] Specifically, the tailoring of surface chemistry with high spatial resolution will be enabling for many graphene-based electronic and sensor applications.

Conductive atomic force microscope (cAFM) nanolithography is a versatile technique for nanopatterning semiconducting and metallic surfaces in a variety of environments including air and organic solvents.[9,10] In its most common form, a positive bias is applied to the sample with respect to the grounded cAFM tip, leading to local anodic oxidation within the water meniscus at the tip–sample junction.[11–24] The local chemical contrast between the oxide nanopatterns and the remainder of the sample surface has been exploited to template subsequent selective attachment of organic and biological molecules.[9]

Recently, cAFM has been employed for nanopatterning of carbon-based materials including carbon nanotubes,[25] mechanically exfoliated graphene flakes,[26–28] epitaxial graphene on silicon carbide,[29] highly oriented pyrolytic graphite (HOPG),[30,31] and graphene oxide.[32] In particular, the initial studies on graphene[26–29] have focused on the utility of cAFM nanopatterning for fabricating prototype electronic devices from graphene nanoribbons. However, the cAFM nanopatterning kinetics, growth mechanism, and chemistry on graphene remain open questions. In this report, we address these issues by quantifying the kinetics and etching of cAFM nanopatterning on EG on SiC(0001). These measurements suggest that cAFM nanopatterning leads to local oxidation with a non-uniform depth profile dictated by the surface, interface, and bulk of the EG/SiC substrate. Finally, cAFM nanopatterning on partially graphitized SiC(0001) is shown to induce highly anisotropic lateral growth that further illustrates the chemical and electronic property differences between EG and SiC. Overall, this study provides quantitative insight into the nanoscale chemical modification of graphene by cAFM, thus informing future efforts to fabricate and test prototype graphene-based electronic and sensing devices.

Preparation of the EG/SiC samples and subsequent scanning tunneling microscopy (STM) characterization were conducted in a home-built ultrahigh vacuum (UHV) system[33] (see Supporting Information). The degree of graphitization was controlled, with fully graphitized samples possessing domains of single-layer graphene (SLG) and bilayer graphene (BLG), and partially graphitized samples possessing domains of SLG, BLG, and exposed regions of an interfacial layer with a carbon-rich $(6\sqrt{3} \times 6\sqrt{3})$ R30° surface reconstruction, typically called the $6\sqrt{3}$ layer (see Figure S1, Supporting Information).

Figure 1 shows AFM topography images of the EG/SiC surface after ambient cAFM nanopatterning at various dwell times and applied biases. Reproducible and uniform patterns of arbitrary geometry can be generated by precisely controlling the applied bias, position, and velocity of the cAFM tip. In Figure 1a, the highest spatial resolution feature is nanopatterned at 6 V for 0.1 s, leading to a height of ≈1.2 nm and an apparent width of ≈36 nm. Considering the relative humidity (≈35%) and hydrophilic nature of the silicon tip, this feature size is comparable to cAFM nanopatterning on other surfaces (e.g., hydrogen-passivated silicon) where the spatial resolution is dictated by the size of the water meniscus at the tip–sample junction.[34] Indeed, we observe a general increase in the size of the patterned features with increasing humidity (see Figure S2, Supporting Information). In Figure 1b, nanostructures were created by varying the applied bias while the tip dwell time was held constant. The threshold voltage for nanopatterning is 5 ± 0.5 V. In Figure 1c, lines are uniformly written across substrate atomic step edges, while in Figure 1d, "Graphene/SiC" is written on the surface to demonstrate the geometric flexibility of cAFM nanopatterning on graphene.

The growth kinetics of cAFM nanopatterning on EG/SiC were studied as a function of applied voltage and write speed. The height values were extracted from multiple topographic cross-sections taken along nanopatterned lines. Since the nanopatterned lines typically cross multiple atomic steps in the

J. M. P. Alaboson, Q. H. Wang, J. A. Kellar, J. Park, Prof. M. C. Hersam
Department of Materials Science and Engineering
Northwestern University
2220 Campus Drive, Evanston, IL 60208, USA
E-mail: m-hersam@northwestern.edu
J. M. P. Alaboson, Dr. M. J. Pellin
Materials Science Division
Argonne National Laboratory
9700 S. Cass Avenue, Argonne, IL 60439, USA
Dr. J. W. Elam
Energy Systems Division
Argonne National Laboratory
9700 S. Cass Avenue, Argonne, IL 60439, USA

DOI: 10.1002/adma.201100367

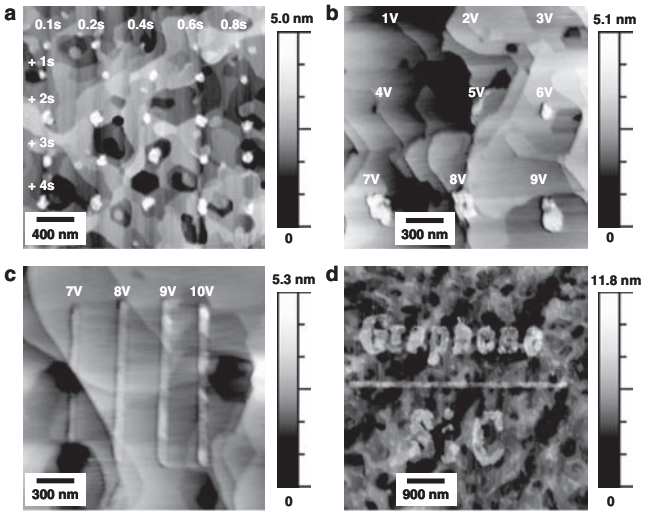

Figure 1. Nanopatterning of epitaxial graphene on SiC. a) AFM image of a grid of cAFM nanopatterns. During cAFM nanopatterning, the sample voltage was held constant at 6 V, while the dwell time was varied from 0.1 s to 4.8 s as indicated in the figure. b) AFM image of a grid of cAFM nanopatterns created by varying the voltage from 1 V to 9 V, while the dwell time was held constant at 4 s. c) AFM image of linear cAFM nanopatterns. The voltage was varied from 7 V to 10 V, while the tip speed was held constant at 1 μm s^{-1}. d) cAFM nanopattern that spells "Graphene/SiC." Nanopatterning was conducted at a constant bias of 9 V and a tip speed of 1 μm s^{-1}. All cAFM nanopatterning in this figure was conducted at ≈35% relative humidity.

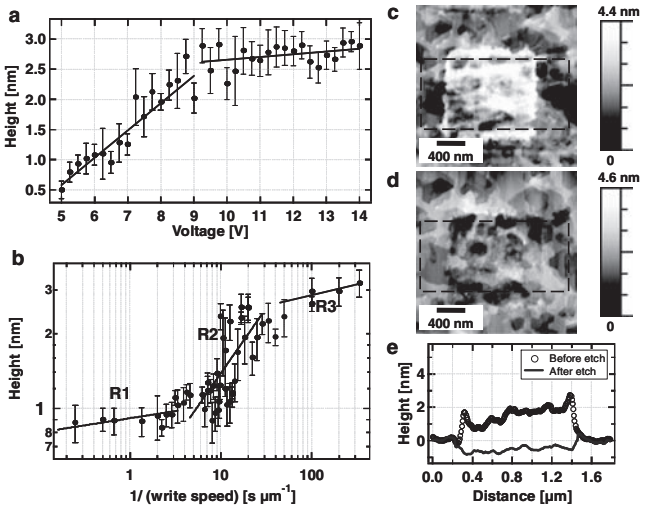

Figure 2. Kinetics and chemical etching of cAFM nanopatterns. a) A plot of cAFM nanopattern height as a function of applied sample bias. The write speed was held constant at 0.25 μm s^{-1}. Solid lines show linear fits over two distinct regimes (5–9 V and 9–14 V). b) A log–log plot of cAFM nanopattern height as function of the inverse write speed. The sample voltage was held constant at 7 V. Solid lines show linear fits over the three distinct regimes labeled in the figure. All data in this figure were gathered at ≈35% relative humidity. c) AFM image of a cAFM nanopatterned box before HF etching. Nanopatterning was achieved by scanning a box at a sample bias of 10 V and a constant tip speed of 1 μm s^{-1}. d) AFM image of the same region after HF etching for 20 min. e) A plot of the line profiles averaged over the indicated boxes before and after HF etching.

underlying substrate, each height measurement was performed with respect to the atomically flat graphene terrace for that cross-section of the nanopatterned line. Following repeated application of this procedure along the nanopatterned line, the mean and standard deviation (depicted with error bars) of the height were found for each nanopatterning condition. In **Figure 2**a, the nanopattern height is plotted versus the applied voltage between 5 V and 14 V at a constant write speed of 0.25 μm s^{-1}. These bias-dependent data follow two linear trends with different slopes: a relatively steep slope between 5 V and 9 V and a shallower slope above 9 V. In Figure 2b, the nanopattern height is plotted versus the inverse of write speed with the applied bias held constant at 7 V. These time-dependent data can be categorized into three distinct regimes on a log–log plot. Within each regime, a line can be fit to an empirical kinetic expression of the form, $z = \alpha\,(\upsilon_0/\upsilon_{ox})^{\gamma}$,[16] where z is the nanopattern height, υ_{ox} is the write speed, υ_0 is an arbitrary constant, and α and γ are fitting parameters. In the initial stages of growth (labeled R1), the nanopattern height shows relatively slow kinetics until the inverse write speed reaches ≈5 s μm^{-1} at which point the growth progresses rapidly (labeled R2). In particular, the fitting parameter γ changes by an order of magnitude from a value of 0.05 ± 0.02 in region R1 to a value of 0.53 ± 0.11 in region R2. Finally, at an inverse speed of ≈40 s μm^{-1} (labeled R3), growth slows down again to a value of $\gamma = 0.1 \pm 0.06$.

The samples were etched in hydrofluoric acid (HF) to investigate the chemical nature of the features created by cAFM nanopatterning. Figure 2c is an AFM image after fabrication of a nanopatterned box, and Figure 2d is the same region after etching in HF. The average height profiles before and after etching are shown in Figure 2e. The depression after etching is consistent with oxidation of the substrate, which is well-established for local anodic oxidation of silicon.[12,13]

To further explore cAFM nanopatterning as a function of substrate composition, experiments were performed on partially graphitized SiC, where graphene coexists with surface regions of ungraphitized 6√3 domains. In a recent study, we established that the ungraphitized 6√3 domains can be spatially mapped and distinguished from graphene using cAFM.[35] In particular, a strong contrast is detected in the current through the cAFM tip with the graphene domains showing substantially higher current than the ungraphitized 6√3 domains. For example, **Figure 3**a,b show topography and current maps, respectively, of the same region of a partially graphitized SiC sample. The regions of markedly lower current are attributed to the ungraphitized 6√3 domains in accordance with a previous study.[35] While cAFM nanopatterning can be achieved on both the ungraphitized 6√3 and graphene domains, lateral nanopattern growth occurs preferentially on graphene. In particular, Figure 3c,d show the topography and current map, respectively, after cAFM nanopatterning was performed on graphene at point "A", in the vicinity of surrounding 6√3 domains marked by regions "B" and "C". At elevated relative humidity (≈50%) and a nanopatterning dwell time of 10 s, significant lateral nanopatterning occurs in a highly anisotropic manner that is confined to the graphene regions while avoiding the 6√3 domains. Consistent with the formation of an oxide, the nanopattern shows low current in the post-nanopatterning cAFM current map.

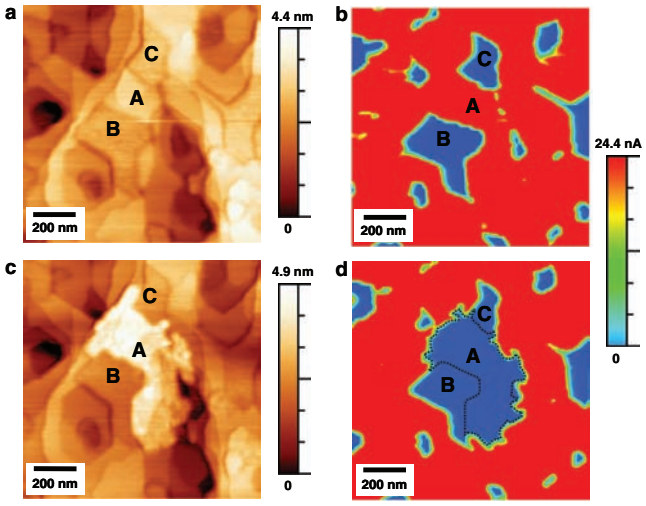

Figure 3. Nanopatterning on partially graphitized SiC. a) Topographic and b) current cAFM images of a partially graphitized SiC substrate preceding nanopatterning. The low current regions are ungraphitized 6√3 domains. c) Topographic and d) current cAFM images after nanopatterning at the point marked by an "A". "B" and "C" mark two 6√3 regions that remain unchanged before and after nanopatterning. Anisotropic lateral growth is confined to graphene and avoids the ungraphitized 6√3 domains. Patterning in this image was accomplished at ≈50% relative humidity. Current maps were taken at a sample bias of 0.3 V.

The dependence of the cAFM nanopattern height on sample bias and dwell time shown in Figure 1,2 suggests that the mechanism of cAFM nanopatterning on EG/SiC is most likely local anodic oxidation within the water meniscus at the tip–sample junction. This interpretation is supported by the observation that nanopatterning is only possible at positive sample bias in this work, which is in agreement with published reports of local anodic oxidation of exfoliated graphene and HOPG.[26–28,30,31] Furthermore, the nanopattern lateral size is observed to increase with increasing relative humidity (see Figure S2, Supporting Information), which has been widely observed in previous studies of AFM local anodic oxidation and most commonly attributed to the increasing size of the water meniscus at the tip–sample junction at elevated humidity.[11–13] The kinetics and chemistry (indicated by HF etching) of the cAFM nanopatterns on EG/SiC also share qualitative similarities to local anodic oxidation on other substrates such as silicon.[11–13]

While local anodic oxidation is the likely overarching mechanism, a closer inspection reveals many unique features of cAFM nanopatterning on EG/SiC. For example, in Figure 1b, the dots nanopatterned at biases above 7 V show anisotropic structure laterally even though the surface was fully graphitized in this case. We believe that this anisotropic structure can be attributed to subtle chemical reactivity and surface energy differences between SLG and BLG as has been observed previously for other reactions including hydrogenation[36] and oxidative etching.[37]

The kinetics of cAFM nanopatterning on EG/SiC show clear differences compared to the canonical example of silicon. In particular, the bias and time dependence of the cAFM nanopattern height in Figure 2 shows distinct regimes that can be attributed to the layered structure of EG/SiC.[38] As the cAFM nanopattern grows thicker and correspondingly oxidizes deeper into the substrate, the growth front first passes through the graphene surface layer, then through the carbon-rich 6√3 interfacial layer, and ultimately into the bulk SiC substrate. Unlike silicon where the chemical composition is essentially identical with depth, the chemically inhomogeneous depth profile of the EG/SiC substrate likely explains the more complicated kinetics observed in Figure 2. We attribute the spread in the kinetics data to the spatially varying interface structure of UHV-processed epitaxial graphene on SiC and to the different local anodic oxidation rates of SLG and BLG as has been previously observed for exfoliated graphene flakes on SiO_2.[27] While the etching behavior of the nanopatterns on EG/SiC in HF is similar to that of anodically oxidized silicon,[12,13] we expect a dependence of the cAFM nanopattern chemistry on the nanopattern height due to the inequivalent oxidation stoichiometry and structure of the graphene surface, 6√3 interface, and SiC bulk.[39–44]

The differences in chemistry, surface energy, and electrical properties between graphene and SiC are further highlighted by the strongly anisotropic lateral growth observed on partially graphitized SiC. As shown in Figure 3, lateral growth is confined to graphene and avoids the 6√3 domains when cAFM nanopatterning is initiated on a graphene portion of partially graphitized SiC. At least two factors may contribute to this unique anisotropic lateral growth mode. First, local anodic oxidation is known to vary with tip–sample conductivity and nanopatterning current.[11] Hence, the substantially higher tip–sample conductivity (indicated by the cAFM current map in Figure 3b) on graphene compared to the 6√3 domains implies preferential anodic oxidation of graphene. Second, from macroscopic water contact angle measurements on 6√3 silicon carbide and epitaxial graphene samples (see Figure S3, Supporting Information), we find the 6√3 surface to be more hydrophobic (average water contact angle = 76°) than fully graphitized SiC samples (average water contact angle = 64°). This contrast in surface energy suggests that the water meniscus at the tip–sample junction may be preferentially confined to graphene, thus leading to selective anodic oxidation of graphene on partially graphitized SiC.

In summary, cAFM nanopatterning has been demonstrated and quantified for EG/SiC in ambient conditions. With many qualitative similarities to other well-established substrates, the overarching cAFM nanopatterning mechanism on EG/SiC appears to be local anodic oxidation. However, detailed quantification of the nanopatterning kinetics reveals subtle differences that can be attributed to the multilayer, chemically inhomogeneous surface and sub-surface structure of EG/SiC. Furthermore, anisotropic lateral growth illustrates that cAFM nanopatterning is also sensitive to lateral inhomogeneities in electrical conductivity and surface energy, especially for partially graphitized SiC substrates where graphene is in direct lateral proximity with 6√3 domains. Since cAFM nanopatterning in ambient conditions is a common pathway for prototyping nanoscale devices and circuits, this study is likely to impact ongoing efforts to understand and optimize the performance of graphene-based electronic and sensing technologies.

Experimental Section

AFM Nanopatterning: AFM measurements were carried out using a modified CP Research (Thermomicroscopes) AFM. Nanopatterning was performed in a controlled-humidity glove box using a Si tip (μMasch, NSC36C). The relative humidity was varied between 20% and 50%. All experiments were performed at room temperature, and the temperature of the tip and substrate were not independently controlled. Height measurements were extracted from AFM images taken in contact mode (fast *y*-scan direction) or intermittent-contact mode to prevent distortion arising from crosstalk between vertical and lateral forces.[45] Chemical etching of the cAFM nanopatterns was performed by dipping the samples in 48% hydrofluoric acid (Aldrich) for 20 min. The same regions were imaged before and after etching with AFM.

Conductive AFM: Current mapping was achieved with a Pt-coated Si probe (μMasch, NSC36C Ti/Pt) in contact mode with contact forces of ≈8–15 nN, a scan rate of 0.3 Hz, and a sample bias of 0.3 V. Current was collected through the cAFM probe using a DL Instruments current preamplifier (Model 1212) and a 160 Hz low-pass in-line filter. A limiting resistor (≈12 MΩ) was used in series with the current preamplifier to limit the maximum current through the cAFM tip. The cAFM probes were tested on Au reference samples, where contact resistances of <5 kΩ were recorded. Contact mode topography signals were collected concurrently with the current signal.

Supporting Information

Supporting Information is available from the Wiley Online Library or from the author.

Acknowledgements

This work was supported by the National Science Foundation (Award Numbers EEC-0647560 and DMR-0520513), the Army Research Office (Award Number ARO W911NF-05–1-0177), and Argonne National Laboratory (ANL). ANL is a U.S. Department of Energy Office of Science Laboratory operated under Contract No. DE-AC02–06CH11357 by UChicago Argonne, LLC. The authors also thank Joseph Lyding for use of his STM control software.

Received: January 28, 2011
Revised: February 16, 2011
Published online: March 7, 2011

[1] A. K. Geim, *Science* **2009**, *324*, 1530.
[2] C. Berger, Z. M. Song, X. B. Li, X. S. Wu, N. Brown, C. Naud, D. Mayou, T. B. Li, J. Hass, A. N. Marchenkov, E. H. Conrad, P. N. First, W. A. de Heer, *Science* **2006**, *312*, 1191.
[3] W. A. de Heer, C. Berger, X. S. Wu, P. N. First, E. H. Conrad, X. B. Li, T. B. Li, M. Sprinkle, J. Hass, M. L. Sadowski, M. Potemski, G. Martinez, *Solid State Commun.* **2007**, *143*, 92.
[4] J. Kedzierski, P. L. Hsu, P. Healey, P. W. Wyatt, C. L. Keast, M. Sprinkle, C. Berger, W. A. de Heer, *IEEE Trans. Electron Devices* **2008**, *55*, 2078.
[5] E. Bekyarova, M. E. Itkis, P. Ramesh, C. Berger, M. Sprinkle, W. A. de Heer, R. C. Haddon, *J. Am. Chem. Soc.* **2009**, *131*, 1336.
[6] Q. H. Wang, M. C. Hersam, *Nat. Chem.* **2009**, *1*, 206.
[7] X. R. Wang, S. M. Tabakman, H. J. Dai, *J. Am. Chem. Soc.* **2008**, *130*, 8152.
[8] D. B. Farmer, H. Y. Chiu, Y. M. Lin, K. A. Jenkins, F. N. Xia, P. Avouris, *Nano Lett.* **2009**, *9*, 4474.
[9] R. Garcia, R. V. Martinez, J. Martinez, *Chem. Soc. Rev* **2006**, *35*, 29.
[10] C. R. Kinser, M. J. Schmitz, M. C. Hersam, *Nano Lett.* **2005**, *5*, 91.
[11] P. Avouris, R. Martel, T. Hertel, R. Sandstrom, *Appl. Phys. A.* **1998**, *66*, S659.
[12] P. Avouris, T. Hertel, R. Martel, *Appl. Phys. Lett.* **1997**, *71*, 285.
[13] M. J. Schmitz, C. R. Kinser, N. E. Cortes, M. C. Hersam, *Small* **2007**, *3*, 2053.
[14] A. E. Gordon, R. T. Fayfield, D. D. Litfin, T. K. Higman, *J. Vac. Sci. Technol., B* **1995**, *13*, 2805.
[15] E. Dubois, J. L. Bubendorff, *J. Appl. Phys.* **2000**, *87*, 8148.
[16] T. Teuschler, K. Mahr, S. Miyazaki, M. Hundhausen, L. Ley, *Appl. Phys. Lett.* **1995**, *67*, 3144.
[17] D. Stievenard, P. A. Fontaine, E. Dubois, *Appl. Phys. Lett.* **1997**, *70*, 3272.
[18] E. S. Snow, G. G. Jernigan, P. M. Campbell, *Appl. Phys. Lett.* **2000**, *76*, 1782.
[19] J. A. Dagata, T. Inoue, J. Itoh, H. Yokoyama, *Appl. Phys. Lett.* **1998**, *73*, 271.
[20] J. A. Dagata, F. Perez-Murano, C. Martin, H. Kuramochi, H. Yokoyama, *J. Appl. Phys.* **2004**, *96*, 2386.
[21] R. Garcia, M. Calleja, F. Perez-Murano, *Appl. Phys. Lett.* **1998**, *72*, 2295.
[22] S. Gomez-Monivas, J. J. Saenz, M. Calleja, R. Garcia, *Phys. Rev. Lett.* **2003**, *91*, 056101.
[23] J. A. Dagata, T. Inoue, J. Itoh, K. Matsumoto, H. Yokoyama, *J. Appl. Phys.* **1998**, *84*, 6891.
[24] J. A. Dagata, F. Perez-Murano, G. Abadal, K. Morimoto, T. Inoue, J. Itoh, H. Yokoyama, *Appl. Phys. Lett.* **2000**, *76*, 2710.
[25] D. H. Kim, J. Y. Koo, J. J. Kim, *Phys. Rev. B* **2003**, *68*, 113406.
[26] A. J. M. Giesbers, U. Zeitler, S. Neubeck, F. Freitag, K. S. Novoselov, J. C. Maan, *Solid State Commun.* **2008**, *147*, 366.
[27] S. Masubuchi, M. Ono, K. Yoshida, K. Hirakawa, T. Machida, *Appl. Phys. Lett.* **2009**, *94*, 082107.
[28] L. S. Weng, L. Y. Zhang, Y. P. Chen, L. P. Rokhinson, *Appl. Phys. Lett.* **2008**, *93*, 093107.
[29] G. Rius, N. Camara, P. Godignon, F. Perez-Murano, N. Mestres, *J. Vac. Sci. Technol., B* **2009**, *27*, 3149.
[30] Y. Jiang, W. L. Guo, *Nanotechnology* **2008**, *19*, 345302.
[31] J. G. Park, C. Zhang, R. Liang, B. Wang, *Nanotechnology* **2007**, *18*, 405306.
[32] Z. Q. Wei, D. B. Wang, S. Kim, S. Y. Kim, Y. K. Hu, M. K. Yakes, A. R. Laracuente, Z. T. Dai, S. R. Marder, C. Berger, W. P. King, W. A. de Heer, P. E. Sheehan, E. Riedo, *Science* **2010**, *328*, 1373.
[33] E. T. Foley, N. L. Yoder, N. P. Guisinger, M. C. Hersam, *Rev. Sci. Instrum.* **2004**, *75*, 5280.
[34] C. R. Kinser, M. J. Schmitz, M. C. Hersam, *Adv. Mater.* **2006**, *18*, 1377.
[35] J. A. Kellar, J. M. P. Alaboson, Q. H. Wang, M. C. Hersam, *Appl. Phys. Lett.* **2010**, *96*, 143103.
[36] S. Ryu, M. Y. Han, J. Maultzsch, T. F. Heinz, P. Kim, M. L. Steigerwald, L. E. Brus, *Nano Lett.* **2008**, *8*, 4597.
[37] L. Liu, S. M. Ryu, M. R. Tomasik, E. Stolyarova, N. Jung, M. S. Hybertsen, M. L. Steigerwald, L. E. Brus, G. W. Flynn, *Nano Lett.* **2008**, *8*, 1965.
[38] J. Hass, J. E. Millan-Otoya, P. N. First, E. H. Conrad, *Phys. Rev. B* **2008**, *78*, 205424.
[39] W. W. Cai, R. D. Piner, F. J. Stadermann, S. Park, M. A. Shaibat, Y. Ishii, D. X. Yang, A. Velamakanni, S. J. An, M. Stoller, J. H. An, D. M. Chen, R. S. Ruoff, *Science* **2008**, *321*, 1815.
[40] W. S. Hummers, R. E. Offeman, *J. Am. Chem. Soc.* **1958**, *80*, 1339.
[41] T. Nakajima, A. Mabuchi, R. Hagiwara, *Carbon* **1988**, *26*, 357.
[42] T. Nakajima, Y. Matsuo, *Carbon* **1994**, *32*, 469.
[43] C. Raynaud, *Non-Cryst. Solids* **2001**, *280*, 1.
[44] I. Vickridge, J. Ganem, Y. Hoshino, I. Trimaille, *J. Phys D: Appl. Phys.* **2007**, *40*, 6254.
[45] M. W. Such, D. E. Kramer, M. C. Hersam, *Ultramicroscopy* **2004**, *99*, 189.